Defect states dependence of spin transport in iron phthalocyanine spin valves

Junwei Tong, Liuxia Ruan, Xiannian Yao, Gaowu Qin, and Xianmin Zhang*
Key Laboratory for Anisotropy and Texture of Materials (Ministry of Education), School of Material Science and Engineering, Northeastern University, Shenyang 110819, China

(Received 12 November 2018; revised manuscript received 25 January 2019; published 7 February 2019)

We fabricated spin-valve devices with a Co/iron phthalocyanine (FePc)/Co stacking structure. The spin-transport properties were systemically studied by varying the measurement temperature and magnetoresistance was confirmed. The estimated value of the spin-diffusion length for the FePc layer is around 30 nm. The existence of defect states was demonstrated based on the analysis of current-voltage curves. Carrier mobilities in the devices were calculated following a trap-filled space charge limited current model, showing the mobility could be up to $2.95 \times 10^{-5}\,\mathrm{cm}^2/\mathrm{Vs}$ at 290 K. The molecular orientation growth of FePc on Co and the interfacial interaction for FePc/Co are also discussed. This work deepens the understanding of spin transport in organic spin devices.

DOI: 10.1103/PhysRevB.99.054406

Investigations on the mechanism of spin injection, transport, and detection as well as interface coupling have made impressive progress in organic spin valves (OSVs) [1–6]. The transport behavior, including diffusion, as well as single-step tunneling or multistep tunneling in disordered organic semiconductors (OSC) have been proposed [7–11]. It has been reported that the site-energy disorder or positional disorder, spin mixing, and exchange coupling between localized polarons contribute to the spin transport [12–15]. In most cases, the semiconductor films are of an amorphous structure, which unavoidably gives rise to defects [16–20]. Although defect states as trap levels affect spin transport in OSVs [21–24], special studies about the effect of defect states on spin-conserved transport are rare. Rybicki *et al.* reports that the traps lead to a dramatic decrease of spin-diffusion length in organic spintronic devices [25]. Conversely, Yu suggests that a high defect density impurity band is responsible for charge/spin transport in the OSVs [26]. Thus, the role of defects is vital for further understanding organic spintronics.

Metal phthalocyanines (Pcs) have drawn considerable attention for efficient spin transport in organic spintronics because of their electronic delocalization [27–30]. Cinchetti *et al.* demonstrated the possibility of spin injection from Co into CuPc using spin-resolved two-photon photoemission [31]. However, reports about the magnetoresistance (MR) effect in OSVs using Pcs as spacers are still contradictory. Wu *et al.* reported that the spin-diffusion length in CuPc-based OSVs mainly depends on the spin-orbit interaction, rather than crystal structure [32]. Majumdar *et al.* found that fast spin relaxation inside the CoPc layer due to the presence of heavy Co atoms, interface coupling of the molecule with electrodes, and associated strong spin-orbit coupling make CoPc unsuitable for spin devices [33,34]. In our opinion, defects generally appear in Pc films, which should be considered in spin transport. Among the Pcs, FePc was predicted to have an excellent spin filter effect [35–37], which is promising for organic spintronic applications. The charge transfer from nonmagnetic metal substrates to FePc molecules has been demonstrated [38,39]. The interface hybridizations for FePc molecules with Co substrate were systematically investigated, which govern the spin injection from the Co into the FePc layer [40–42]. Although the above impressive progress has been made, the OSV device using the FePc layer has not been reported.

In this paper, we report the fabrication of OSV with a glass-substrate/Co/FePc/Co/Al stacking structure prepared without breaking the vacuum condition. MR in the present devices was systemically studied by varying the measurement temperatures. The existence of defect states was confirmed based on the analysis of current-voltage curves. Carrier mobilities were calculated following a trap-filled space charge limited current model, showing carrier mobility could be up to $2.95 \times 10^{-5}\,\mathrm{cm}^2/\mathrm{Vs}$ at 290 K. The molecular orientation of FePc on Co and interfacial interaction for FePc/Co are discussed.

The spin-valve device with a vertical sandwiched structure is shown in Fig. 1(a). The electrical current through our device was perpendicular to the deposited films, and the magnetic field H was applied parallel to the films. Both the bottom and top electrode were prepared by a magnetron sputtering, while the FePc layer was deposited by a thermal evaporation. It should be noted that the sputtering power was only 10 W to avoid or reduce metallic inclusion into the OSC layer when depositing the top electrode. Prior to deposition, the glass substrates were ultrasonically cleaned with acetone, ethanol, and deionized water in sequence. The base pressure for deposition was $1 \times 10^{-6}\,\mathrm{Pa}$, while the pressure for sputtering and evaporation was 0.2 Pa and $\sim 2\text{–}5 \times 10^{-4}\,\mathrm{Pa}$, respectively. First, the bottom Co electrode with a film thickness of about 50 nm was prepared by using a shadow mask. Then we deposited a FePc stripe onto the bottom Co electrode by changing the shadow mask. 10 nm Al was deposited to prevent oxidation of the Co top layer (30 nm). The top Co/Al layer was deposited by the third shadow mask. The whole

*zhangxm@atm.neu.edu.cn

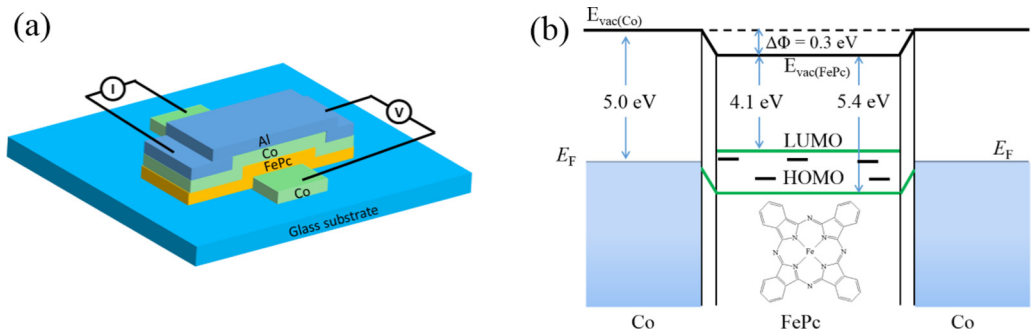

FIG. 1. (a) Schematic diagram of the device structure with a glass substrate/Co/FePc/Co/Al stacking structure. (b) Schematic band diagram of the organic device in the rigid band diagram shows the Fermi levels (E_F), the work function of the ferromagnetic electrode Co, and the HOMO and LUMO levels of FePc. $\Delta\Phi$ means the difference of work functions between Co and FePc. The short lines between the HOMO and LUMO levels depict possible defect states within the FePc layer.

fabrication procedure was completed without breaking the vacuum. The active device area was about 2×2 mm. The film thicknesses were controlled by a quartz-crystal resonator. The MR curves were measured via a standard four-probe method using a physical property measurement system (Quantum Design) at temperatures between 10 and 300 K. The electrical measurements were performed with a ECOPIA HMS-5000 at the range of 80 to 290 K. The crystal structures of the films were measured by using a powder x-ray diffractmeter (Japan Rigaku X-ray) of Cu Kα radiation in the range of 5–20°. The magnetization curves were measured using a vibrating sample magnetometer (Lakeshore 7400).

The highest occupied molecular orbital (HOMO) and lowest unoccupied molecular orbital (LUMO) of FePc lie about 0.7 eV below and 0.6 eV above the Fermi levels (E_F) of the Co electrodes, respectively [43,44]. The work function of Co was about 5 eV [3]. Thus, the energy diagram of Co/FePc/Co is drawn in Fig. 1(b). The possible defect states in the FePc layer are also indicated in Fig. 1(b), which may affect spin transport [21–26].

Figure 2(a) shows typical MR curves of the Co/FePc (50 nm)/Co devices measured at the bias current of 10^{-4} mA. The OSV clearly exhibits a positive MR at all measurement temperatures (10, 50, and 100 K). The MR ratio is defined as $\mathrm{MR} = (R_{AP} - R_P)/R_P$, where R_{AP} and R_P are the resistance of the two ferromagnetic (FM) electrodes in the antiparallel and parallel configurations, respectively. The calculated MR ratio is around 4%, 1.2%, and 0.5% at 10, 50, and 100 K, respectively. The dependence of the device resistance in parallel configuration on temperatures is drawn in Fig. 2(b), clearly indicating a linear increase with increasing measurement temperatures. Upon cooling from 300 to 10 K, the device resistance increases around 2.5-fold. Such an increase in resistance with decreasing temperature has been observed for spin vales with various organic barriers [7,10,45–47]. This demonstrates that spin transport is dominated by diffusion, rather than tunneling. To further study the electrical resistance of the OSV device, the corresponding resistance-area (RA) product value with different FePc layer thickness is plotted in Fig. 2(c). Some results in the literature [9,29,48] were also summarized to perform a comparison with the present results. The RA increases with the increase of FePc layer thickness, indicating that the OSV devices are pinhole free and the device resistances are dominated by the organic layer [9,45,46]. Moreover, the present results are in good agreement with the reported values using other Pc spacer layers by other groups owing to their similar molecular structures.

As shown in Fig. 2(b), the maximum of the MR ratio was 4% at $T = 10$ K and vanished above 200 K. The MR ratio drastically decreases with increasing temperature. According to previous reports [7,45–47], the MR of OSVs using 3d transition ferromagnetic electrodes (Fe, Co, Ni, and their alloys) also showed temperature dependence. Since the magnetism of Co does change much at those low temperatures below Tc, the MR ratio decrease with temperature cannot be due to the loss of spin polarization of the FM electrode. Thus, the temperature dependence of the MR ratio is generally attributed to the increase of the spin-relaxation rate in the FePc layer. Assuming that the spin polarization P of Co is 30% [49], one could estimate the spin-diffusion length according to the modified Julliere equation [3],

$$\frac{\Delta R}{R_P} = \frac{2P^2 e^{-d/\lambda_s}}{1 + P^2 e^{-d/\lambda_s}}, \tag{1}$$

where d is the film thickness and λ_s is the spin-diffusion length. The estimated value of λ_s is about 33 nm at 10 K. In fact, the actual film thickness should be smaller than the growth thickness of d because of the presence of the ill-defined layer with 1–2 nm in thickness at the interface [1,3,7] between Co and the OSC (which will be discussed below). So λ_s of FePc will also be shorter than that from the fitted value of 33 nm. In OSC films, carriers propagate mainly via hopping between localized states, and spins flip as they hop from site to site due to spin-orbit coupling. Thus, λ_s strongly relies on the strength of the spin-orbit coupling. The smaller value of λ_s for FePc than that of Alq_3 and C_{60} [1–3] is likely due to the presence of the Fe atoms [15,26].

In order to understand the charge transport process in the FePc layer, electrical transport measurements were performed on the OSV device. As shown in Fig. 3(a), nonlinear current-voltage (I-V) curves were clearly observed at all measurement temperatures (80–290 K). The I-V curves are symmetrical for positive and negative voltages due to the symmetrical energy alignments of FePc and Co [see Fig. 1(b)]. Further, with decreasing measurement temperature, the nonlinear response of I-V became stronger owing to the increase for device

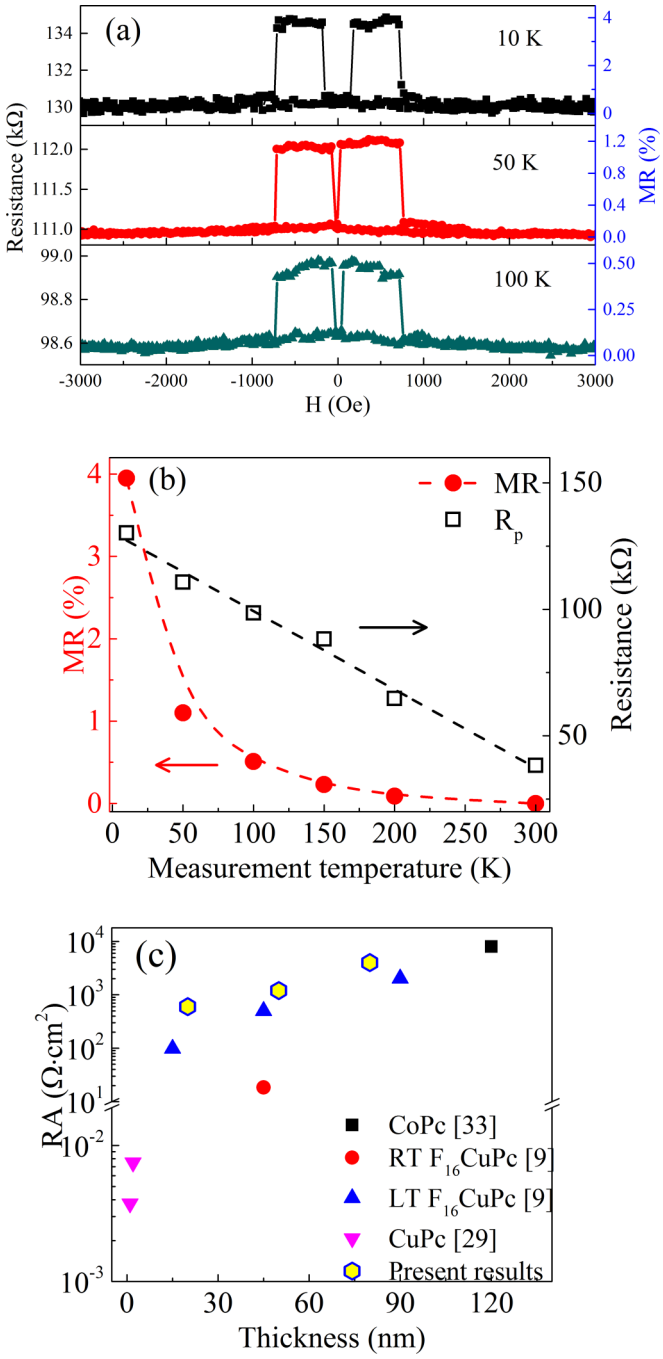

FIG. 2. (a) MR curves of Co/FePc (50 nm)/Co OSV measured at different temperatures with a bias current of 10^{-4} mA. (b) Temperature dependence of resistance (in parallel configurations) and MR for the FePc OSV. (c) Resistance-area product value vs FePc-layer thickness.

resistance at low temperature. Figure 3(b) shows the I-V curves in double logarithmic scale. The I-V curves generally can be discriminated by three distinct regions (regions A, B, and C) depending on the measurement temperatures. The slopes of regions A and C are 1 and 2, which correspond to the ohmic conduction regime and trap-filled space charge limited current regime, respectively [50,51]. The slope of region B is 2.7 at 220 K and 3.5 at 80 K, which is the trap-filling regime [50,51]. A main critical voltage (labeled by circles) shifts to a higher-voltage side with the decrease of measurement temperatures. At lower temperature, three regions could be clearly observed, which means that trap levels should exist in the present FePc film [50–52]. With increasing temperatures, region B gradually disappears. For the results measured at 290 K, only regions A and C appear because the traps were completely filled at a high temperature. With a small voltage (region A), spin-conserved carriers dominantly transport through the energy levels around Fermi level. With increasing applied voltage, the trapping centers between the HOMO and LUMO levels would be gradually occupied by injected charge carriers, resulting in the regions B. With further increase of applied voltage (region C), all the trapping levels were occupied and the injected charge exceeded the intrinsic charge concentration. Thus, the FePc film begins to resist any further injection that the extra injected charges cannot be swept to the collecting electrode with the same rate at which they are being injected. As a result, the slope of region C reduces compared to that of region B.

Such transport behaviors can be attributed to a trap-filled space charge limited current mechanism [50,53]. This can be described by the following formula [50]:

$$J = 9/8\varepsilon_0\varepsilon_r\mu V^2/d^3, \tag{2}$$

where J is the current density, ε_0 is the permittivity of vacuum, $\varepsilon_r = 3.7$ is the relative permittivity of FePc [54], and d is the film thickness. The dependence of mobility on measurement temperatures was plotted in Fig. 3(c). The hole mobility is estimated to be 2.95×10^{-5} cm^2/Vs at 290 K, which is very close to the reported value [55], indicating that the present FePc films are of very high carrier mobility. The high carrier mobility demonstrates that the number of defects is small in the present FePc film. Moreover, the FePc powder for evaporation is free of impurities within the resolution of x-ray diffraction (XRD) and Fourier transform infrared spectrometer [56]. So the defects are very likely not from organic impurities. It was reported that diffused metal atoms into the OSCs layer were limited around 2 nm in depth from the experimental investigation [57] and theoretical calculations [58]. Here, a very small sputtering power (only 10 W) was used to deposit the on-top electrode, which should further reduce metallic inclusion into the FePc layer. Therefore, it is deduced that the defects in the present FePc film were dominantly from crystalline disorder because OSCs lack long-range order. Furthermore, the present FePc film with an amorphous structure was verified by the XRD measurement, as shown in Fig. 4(a). To further analyze the trap distributions, the temperature dependence on resistivity is estimated as $R = R_0\exp(E_a/K_BT)$, where E_a is the thermal activation energy and K_B is the Boltzmann's constant. The logarithmic scale of R versus T^{-1} for the FePc film device was plotted in Fig. 3(d). It is noted that there are two linear regions, corresponding to the activation energies of 1.36 and 21.6 meV, respectively. The values are very small compared to that induced by a special x-ray radiation [25]. This implies that both deep and shallow traps appear in the present FePc film, resulting in the appearance of region B in Fig. 3(b), which agrees with the reported results in the literature [51,52].

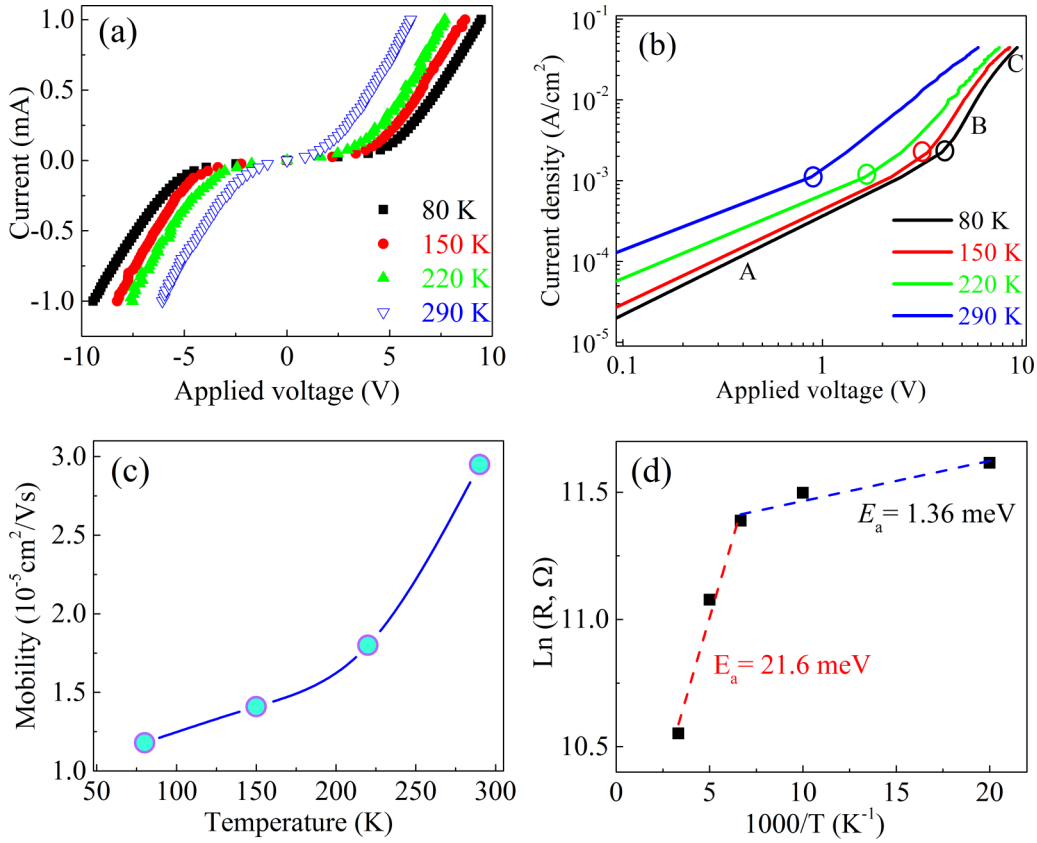

FIG. 3. (a) Current-voltage curves of Co/FePc (50 nm)/Co OSV measured at different temperature (80,150, 220, and 290 K). (b) The double logarithmic scale of current-voltage curves. (c) The dependence of mobility on measurement temperatures. (d) The logarithmic scale of R vs T^{-1} for the FePc film device.

The interface effect between the π electrons of the organic molecule and the 3d electrons of the FM electrode can affect both the crystalline structure of the organic film and the magnetization of the FM metal, which is likely to influence spin transport and injection efficiency [5,59,60]. Figure 4(a) presents the XRD patterns of the FePc films deposited on glass substrates with and without the Co buffer layer. The film of FePc grown directly on the glass substrate exhibits a single sharp peak at 2θ of 6.9°, indicating a polycrystalline structure. However, with the Co buffer layer, the film of FePc did not show any diffraction peak. This is probably due to the chemisorption of the phthalocyanine molecules on the ferromagnetic Co surface, implying FePc molecules are preferred to lie flat [32,61] on the Co surface, as shown in the inset of Fig. 4(a). Moreover, we studied the magnetic properties of Co deposited on glass substrates with and without the FePc

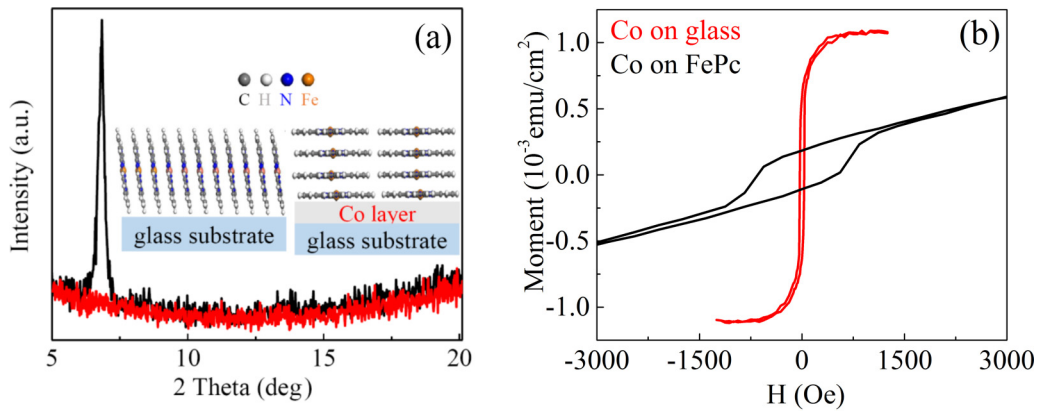

FIG. 4. (a) XRD patterns for FePc deposited on glass substrate (black) and 50 nm Co (red). (b) Hysteresis loops of a Co (30 nm)/Al (10 nm) bilayer (red) and a FePc (50 nm)/Co (30 nm)/Al (10 nm) trilayer (black) measured at room temperature.

insertion layer, as shown in Fig. 4(b). The Co grown directly on the glass substrate shows a coercive field of ∼30 Oe, which is much smaller than that of the FePc buffer sample. Furthermore, the magnetic moment of Co on the FePc layer is drastically suppressed compared to the sample grown directly on glass. This is consistent with the results of CuPc devices reported by Coey *et al.* [29]. It is speculated that the reason for this drastic reduction might be the formation of a magnetic dead layer at the FePc/Co interface. Lach *et al.* also verified that a chemical reaction between the surface Co atoms and FePc molecules could form new hybrid states by spin-resolved photoelectron spectroscopy and band calculations [42]. Moreover, Studniarek *el al.* proposed that the first three Co atomic layers dominated the interface coupling with the FePc film [40]. Such interface interactions could form "spinterfaces," which would be highly important for the future development of new spintronic devices [5,11,60,62].

In summary, spin transport in Co/FePc/Co OSV was studied. MR showed drastic temperature dependence. The spin-diffusion length in the FePc layer was dominantly affected by spin-orbit coupling in the FePc layer. It was also found that both the crystalline structure of the organic film and the magnetization of the ferromagnetic electrode were affected by strong interface interactions, which is likely to influence spin transport and injection efficiency. Defects in the amorphous FePc film were demonstrated and the effect for the spin-conserved transport process was discussed. This study is valuable to design future flexible spin-electronic devices.

This work was supported by the National Natural Science Foundation of China (Grants No. 51471046 and No. 51525101) and the Research Funds for the Central Universities (Grants No. N170205001 and No. N160208001).

[1] D. Sun, E. Ehrenfreund, and Z. V. Vardeny, Chem. Commun. **50**, 1781 (2014).
[2] J. Devkota, R. Geng, R. C. Subedi, and T. D. Nguyen, Adv. Funct. Mater. **26**, 3881 (2016).
[3] Z. H. Xiong, D. Wu, Z. V. Vardeny, and J. Shi, Nature (London) **427**, 821 (2004).
[4] V. Dediu, M. Murgia, F. Matacotta, C. Taliani, and S. Barbanera, Solid State Commun. **122**, 181 (2002).
[5] K. V. Raman, A. M. Kamerbeek, A. Mukherjee, N. Atodiresei, T. K. Sen, P. Lazic, V. Caciuc, R. Michel, D. Stalke, S. K. Mandal, S. Blugel, M. Munzenberg, and J. S. Moodera, Nature (London) **493**, 509 (2013).
[6] X. Sun, S. Vélez, A. Atxabal, A. Bedoya-Pinto, S. Parui, X. Zhu, R. Llopis, F. Casanova, and L. E. Hueso, Science **357**, 677 (2017).
[7] T. S. Santos, J. S. Lee, P. Migdal, I. C. Lekshmi, B. Satpati, and J. S. Moodera, Phys. Rev. Lett. **98**, 016601 (2007).
[8] J. J. H. M. Schoonus, P. G. E. Lumens, W. Wagemans, J. T. Kohlhepp, P. A. Bobbert, H. J. M. Swagten, and B. Koopmans, Phys. Rev. Lett. **103**, 146601 (2009).
[9] X. Sun, A. Bedoya-Pinto, Z. Mao, M. Gobbi, W. Yan, Y. Guo, A. Atxabal, R. Llopis, G. Yu, Y. Liu, A. Chuvilin, F. Casanova, and L. E. Hueso, Adv. Mater. **28**, 2609 (2016).
[10] X. Zhang, S. Mizukami, T. Kubota, Q. Ma, M. Oogane, H. Naganuma, Y. Ando, and T. Miyazaki, Nat. Commun. **4**, 1392 (2013).
[11] M. Sun and W. Mi, J. Mater. Chem. C **6**, 6619 (2018).
[12] P. A. Bobbert, W. Wagemans, F. W. A. van Oost, B. Koopmans, and M. Wohlgenannt, Phys. Rev. Lett. **102**, 156604 (2009).
[13] N. J. Harmon and M. E. Flatte, Phys. Rev. Lett. **108**, 186602 (2012).
[14] N. J. Harmon and M. E. Flatte, Phys. Rev. Lett. **110**, 176602 (2013).
[15] Z. G. Yu, Phys. Rev. Lett. **106**, 106602 (2011).
[16] M. Cox, P. Janssen, F. Zhu, and B. Koopmans, Phys. Rev. B **88**, 035202 (2013).
[17] J. H. Shim, K. V. Raman, Y. J. Park, T. S. Santos, G. X. Miao, B. Satpati, and J. S. Moodera, Phys. Rev. Lett. **100**, 226603 (2008).
[18] R. C. Roundy and M. E. Raikh, Phys. Rev. B **90**, 241202(R) (2014).
[19] Q. Zhang, L. Chen, W. Jia, Y. Lei, and Z. Xiong, Org. Electron. **39**, 318 (2016).
[20] J. Gao and F. AlTal, Appl. Phys. Lett. **104**, 143301 (2014).
[21] J. W. Yoo, C. Y. Chen, H. W. Jang, C. W. Bark, V. N. Prigodin, C. B. Eom, and A. J. Epstein, Nat. Mater. **9**, 638 (2010).
[22] J.-W. Yoo, H. W. Jang, V. N. Prigodin, C. Kao, C. B. Eom, and A. J. Epstein, Phys. Rev. B **80**, 205207 (2009).
[23] X. Zhang, Q. Ma, K. Suzuki, A. Sugihara, G. Qin, T. Miyazaki, and S. Mizukami, ACS Appl. Mater. Interfaces **7**, 4685 (2015).
[24] J.-Y. Hong, Y.-M. Chang, C.-H. Chuang, K.-S. Li, Y.-C. Jhang, H.-W. Shiu, C.-H. Chen, W.-C. Chiang, and M.-T. Lin, J. Phys. Chem. C **116**, 21157 (2012).
[25] J. Rybicki, R. Lin, F. Wang, M. Wohlgenannt, C. He, T. Sanders, and Y. Suzuki, Phys. Rev. Lett. **109**, 076603 (2012).
[26] Z. G. Yu, Nat. Commun. **5**, 4842 (2014).
[27] M.-S. Liao and S. Scheiner, J. Chem. Phys. **114**, 9780 (2001).
[28] X. Zhang, S. Mizukami, T. Kubota, Q. Ma, H. Naganuma, M. Oogane, Y. Ando, and T. Miyazaki, J. Appl. Phys. **111**, 07B320 (2012).
[29] H. Tokuc, K. Oguz, F. Burke, and J. M. D. Coey, J. Phys. Conf. Ser. **303**, 012097 (2011).
[30] H. Jiang, P. Hu, J. Ye, R. Ganguly, Y. Li, Y. Long, D. Fichou, W. Hu, and C. Kloc, Angew. Chem. Int. Ed. **57**, 10112 (2018).
[31] M. Cinchetti, K. Heimer, J. P. Wustenberg, O. Andreyev, M. Bauer, S. Lach, C. Ziegler, Y. Gao, and M. Aeschlimann, Nat. Mater. **8**, 115 (2009).
[32] S. W. Jiang, P. Wang, B. B. Chen, Y. Zhou, H. F. Ding, and D. Wu, Appl. Phys. Lett. **107**, 042407 (2015).
[33] S. Majumdar, S. Dey, H. Huhtinen, J. Dahl, M. Tuominen, P. Laukkanen, S. Van Dijken, and H. S. Majumdar, Spin **04**, 1440009 (2014).
[34] S. Majumdar, K. Grochowska, M. Sawczak, G. Sliwinski, H. Huhtinen, J. Dahl, M. Tuominen, P. Laukkanen, and H. S. Majumdar, ACS Appl. Mater. Interfaces **7**, 22228 (2015).
[35] Y.-H. Zhou, J. Zeng, L.-M. Tang, K.-Q. Chen, and W. P. Hu, Org. Electron. **14**, 2940 (2013).

[36] X. Shen, L. Sun, Z. Yi, E. Benassi, R. Zhang, Z. Shen, S. Sanvito, and S. Hou, Phys. Chem. Chem. Phys. **12**, 10805 (2010).
[37] C. R. Natoli, P. Krüger, Y. Yoshimoto, J. Bartolomé, and F. Bartolomé, Phys. Rev. B **98**, 195108 (2018).
[38] A. Mugarza, R. Robles, C. Krull, R. Korytár, N. Lorente, and P. Gambardella, Phys. Rev. B **85**, 155437 (2012).
[39] J.-P. Gauyacq, F. D. Novaes, and N. Lorente, Phys. Rev. B **81**, 165423 (2010).
[40] M. Studniarek, S. Cherifi-Hertel, E. Urbain, U. Halisdemir, R. Arras, B. Taudul, F. Schleicher, M. Hervé, C.-H. Lambert, A. Hamadeh, L. Joly, F. Scheurer, G. Schmerber, V. Da Costa, B. Warot-Fonrose, C. Marcelot, O. Mauguin, L. Largeau, F. Leduc, F. Choueikani, E. Otero, W. Wulfhekel, J. Arabski, P. Ohresser, W. Weber, E. Beaurepaire, S. Boukari, and M. Bowen, Adv. Funct. Mater. **27**, 1700259 (2017).
[41] H. C. Herper, S. Bhandary, O. Eriksson, B. Sanyal, and B. Brena, Phys. Rev. B **89**, 085411 (2014).
[42] S. Lach, A. Altenhof, K. Tarafder, F. Schmitt, M. E. Ali, M. Vogel, J. Sauther, P. M. Oppeneer, and C. Ziegler, Adv. Funct. Mater. **22**, 989 (2012).
[43] S. Ahmadi, M. N. Shariati, S. Yu, and M. Gothelid, J. Chem. Phys. **137**, 084705 (2012).
[44] I. E. Brumboiu, S. Haldar, J. Luder, O. Eriksson, H. C. Herper, B. Brena, and B. Sanyal, J. Chem. Theory Comput. **12**, 1772 (2016).
[45] K. Z. Suzuki, T. Izumi, X. Zhang, A. Sugihara, S.-T. Pham, H. Taka, S. Sato, H. Isobe, and S. Mizukami, APL Mater. **5**, 046101 (2017).
[46] M. Gobbi, F. Golmar, R. Llopis, F. Casanova, and L. E. Hueso, Adv. Mater. **23**, 1609 (2011).
[47] I. Martinez, J. P. Cascales, C. Gonzalez-Ruano, J. Y. Hong, C. F. Hung, M.-T. Lin, T. Frederiksen, and F. G. Aliev, J. Phys. Chem. C **122**, 26499 (2018).
[48] A. Banerjee and A. J. Pal, Small **14**, e1801510 (2018).
[49] S. Pramanik, C. G. Stefanita, S. Patibandla, S. Bandyopadhyay, K. Garre, N. Harth, and M. Cahay, Nat. Nanotechnol. **2**, 216 (2007).
[50] Z. Chiguvare and V. Dyakonov, Phys. Rev. B **70**, 235207 (2004).
[51] A. Carbone, B. K. Kotowska, and D. Kotowski, Phys. Rev. Lett. **95**, 236601 (2005).
[52] V. Podzorov, E. Menard, A. Borissov, V. Kiryukhin, J. A. Rogers, and M. E. Gershenson, Phys. Rev. Lett. **93**, 086602 (2004).
[53] V. Coropceanu, J. Cornil, D. A. D. Silva Filho, Y. Olivier, R. Silbey, and J. L. Bredas, Chem. Rev. **107**, 926 (2007).
[54] H. S. Soliman, M. M. El Nahass, A. M. Farid, A. A. M. Farag, and A. A. El Shazly, Eur. Phys. J. Appl. Phys. **21**, 187 (2003).
[55] Z. Bao, A. J. Lovinger, and A. Dodabalapur, Adv. Mater. **9**, 42 (1997).
[56] T. Liu, F. Zhang, L. Ruan, J. Tong, G. Qin, and X. Zhang, Mater. Lett. **237**, 319 (2019).
[57] F. Schmitt, J. Sauther, S. Lach, and C. Ziegler, Anal. Bioanal. Chem. **400**, 665 (2011).
[58] Y.-P. Wang, X.-F. Han, J. N. Fry, J. L. Krause, X. G. Zhang, and H.-P. Cheng, Phys. Rev. B **90**, 075311 (2014).
[59] F. A. Ma'Mari, T. Moorsom, G. Teobaldi, W. Deacon, T. Prokscha, H. Luetkens, S. Lee, G. E. Sterbinsky, D. A. Arena, D. A. MacLaren, M. Flokstra, M. Ali, M. C. Wheeler, G. Burnell, B. J. Hickey, and O. Cespedes, Nature (London) **524**, 69 (2015).
[60] M. Cinchetti, V. A. Dediu, and L. E. Hueso, Nat. Mater. **16**, 507 (2017).
[61] S. Schmaus, A. Bagrets, Y. Nahas, T. K. Yamada, A. Bork, M. Bowen, E. Beaurepaire, F. Evers, and W. Wulfhekel, Nat. Nanotechnol. **6**, 185 (2011).
[62] S. Steil, N. Großmann, M. Laux, A. Ruffing, D. Steil, M. Wiesenmayer, S. Mathias, O. L. A. Monti, M. Cinchetti, and M. Aeschlimann, Nat. Phys. **9**, 242 (2013).